Transactions of Tianjin University (2022) 28:440–445
https://doi.org/10.1007/s12209-022-00314-1

RESEARCH ARTICLE

Fabrication of Ce-ReS_2 by Molten Salt for Electrochemical Hydrogen Evolution

Ran Chen[1] · Minghai Ma[1] · Yi Luo[1] · Liping Qian[1] · Shunli Wan[1] · Shengyou Xu[1] · Xinsong She[1]

Received: 7 January 2022 / Revised: 2 February 2022 / Accepted: 14 February 2022 / Published online: 29 March 2022

Abstract

Renewable and economical generation of hydrogen via electrochemical methods shows great potential in addressing the energy crisis. In this study, an emerging molten salt method was adopted for the synthesis of a cerium-modified rhenium disulfide nanosheet for electrical hydrogen evolution reactions. The prepared 1% Ce-doped rhenium disulfide (ReS_2) sample showed promoted hydrogen evolution performance in both acid and alkaline electrolytes compared to bare ReS_2. Generating of abundant defects in ReS_2 exposed more reaction active sites. Moreover, adding cerium accelerated the hydrogen evolution dynamics. Hopefully, this work will offer new insight into developing ReS_2-based electrocatalysts for hydrogen evolution reactions.

Keywords Hydrogen · Molten salt · Ce-doped rhenium disulfide · Defects

Introduction

Hydrogen production from water splitting via electrochemical methods is considered a potential approach to obtaining renewable energy [1–5]. To date, transition metal dichalcogenides (TMDs) as electrocatalysts have been widely studied for hydrogen evolution reaction (HER) and include MoS_2 [6–8], WS_2 [9–11], $MoSe_2$ [12], WSe_2 [13], and so on. Recently, as a new member of the TMDs, rhenium disulfide (ReS_2) has drawn much attention for its unique, wrinkled **1T** construction, which consists of a unique sinuate Re–Re chain [14]. Meanwhile, the distorted structure of ReS_2 could effectively prevent the accumulation of each layer [15]. Moreover, rhenium disulfide possesses excellent electrical conductivity for the existence of subtle interlamination van der Waals reciprocity [16, 17]. Chen et al. [18] reported a type of few-layered ReS_2 nanosheets grown on graphene for HER via a facile hydrothermal method, and it showed excellent electrocatalytic performance. Additionally, Fujita et al. [19] developed two-dimensional ReS_2 through exfoliation using lithium intercalation. The exfoliated ReS_2 presents a superior HER performance with overpotentials of 100 mV and Tafel plots of 75 mV/dec. The superlattice **1T'** phase of ReS_2 is mainly responsible for the excellent HER performance. Thereafter, the unique structure and excellent conductivity of ReS_2 enable its great potential in electrocatalytic hydrogen production.

However, limited reaction active sites suppress the further application of ReS_2 materials, which are prepared by hydrothermal methods [20]. Meanwhile, only a small amount of ReS_2 can be obtained via hydrothermal methods. Referencing previous reports, synthesizing ReS_2 via a high-temperature solid-state approach is a preferable method on a large scale but suffers from poor electrocatalytic activity [21]. Thereafter, rationally constructing more reaction active sites-exposed ReS_2 electrocatalysts with high performance is crucial for the electrocatalytic HER. Recently, an emerging molten salt approach has attracted much attention as a reformative powder metallurgy technology, which has been widely adopted for synthesizing TMDs [22]. Generally, KSCN is a preferable reagent in molten salt to replace traditional LiCl because it has a lower melting point and is quite stable in the atmosphere, which is served as sulfur (S) source in preparing process [23, 24]. On the base of the above considerations and with the adoption of KSCN as a key ingredient, molten salt shows great potential in preparing TMDs. However, attempts have rarely been directed toward designing high-efficiency ReS_2-based electrocatalysts by molten salt methods for the HER.

✉ Ran Chen
cran@hsu.edu.cn

[1] College of Life & Environmental Sciences, Huangshan University, Huangshan 245041, China

Herein, we prepared few-layered ReS_2 with cerium (Ce)-modified electrocatalysts via molten salt for the HER. KSCN was used as an S source and reaction medium during the preparation of electrocatalysts. The obtained Ce-ReS_2 shows a great HER-boosting effect compared to bare CeS_2. Adding Ce not only provided more active sites but also accelerated the reaction dynamics of the HER.

Experimental

Synthesis of ReS_2

0.3 g H_4NO_4Re and 3 g KSCN were grounded homogeneously. Then, the hybrid solid was calcined in a muffle furnace at 250 °C for 2 h with a heating rate of 5 °C/min. After reaction, the obtained product was washed several times by deionized (DI) water and ethyl alcohol, harvested by centrifugation and dried at 60 °C overnight.

Synthesis of Ce-ReS_2

Ce-ReS_2 samples were fabricated via molten salt method similar to bare ReS_2. 0.3 g H_4NO_4Re, 3 g KSCN and different contents of $Ce(NO_3)_3{\cdot}6H_2O$ were grounded homogeneously. Then, the hybrid solid was calcined in a muffle furnace at 250 °C for 2 h with a heating rate of 5 °C /min. After reaction, the obtained product was washed several times by DI water and ethyl alcohol, harvested by centrifugation and dried at 60 °C overnight. The prepared electrocatalysts were marked as x%Ce-ReS_2 (x% was the molar ratio of $Ce(NO_3)_3{\cdot}6H_2O$ to H_4NO_4Re: 0.5, 1, 2 and 5%). The contents of Ce in x%Ce-ReS_2 are listed in Table S1.

Characterization

X-ray diffraction (XRD) characterization was employed to analyze catalyst structure by a Shimadzu/XD-3A diffractometer system. Copper Kα radiation ($\lambda = 1.5418$ Å) was used. Morphologies of the catalysts were employed through transmission electron microscopy (TEM) by a JEOL 2100 system. X-ray photoelectron spectra (XPS) were carried out by PHI 5000 VersaProbe with Al-Kα radiation. Electron spin-resonance spectroscopy (ESR) was performed by JES FA200. Raman was employed by Bruker senterra. Inductively coupled plasma (ICP) was used by an Agilent 7700 equipment. ICP was employed by an Agilent ICP-MS 7700 equipment.

Electrochemical Measurements

The synthesized catalysts were tested in 0.5 mol/L H_2SO_4 (purged with pure N_2) using a typical three-electrode setup on an electrochemical station (Chenhua Instruments, CHI660D) with a Ag/AgCl reference electrode, a graphite rod as counter electrode and a glassy carbon electrode (GCE) covered with ReS_2 composites as working electrode to study the electrochemical property. Typically, put 5 mg catalysts into a mixed solution with 20 µL Nafion, 245 µL ethyl alcohol and 735 µL water in a centrifuge tube. Then, transfer 60 µL of the as-prepared solution on GCE (radius of 1.5 mm) via pipette carefully before using. The loading amount of the catalyst on GCE was 4.25 mg/cm^2. All potential data are given versus reversible hydrogen electrode (RHE) according to the following equation: Linear sweep voltammetry (LSV) was conducted in 0.5 mol/L H_2SO_4 with a scan rate of 5 mV/s. The current density vs potential data plots were corrected for 90% Ohmic compensation throughout the system. For a Tafel plot, the linear portion fits the Tafel equation to achieve the Tafel slope. Cyclic voltammetry (CV) was measured with scan rates of from 0.01 to 0.10 V for the investigations of electrochemical surface areas. The electrochemical impedance spectroscopy (EIS) measurements were taken with frequencies ranging from 100 kHz to 0.1 Hz. The stability of the catalyst was tested by long-time chronopotentiometry at the current density of 10 mA/cm^2.

Results and Discussion

The as-prepared x%Ce-ReS_2 ($x = 0.5$, 1, 2 and 5) electrocatalysts were obtained via blending H_4NO_4Re, KSCN and $Ce(NO_3)_3{\cdot}6H_2O$, followed by suitable heat treatment in air. Pure ReS_2 was collected for comparison under similar conditions. The contents of Ce in x%Ce-ReS_2 are listed in Table S1. As shown in Fig. S1, XRD patterns of x%Ce-ReS_2 samples keep a similar trend compared to pure ReS_2, illustrating that x%Ce-ReS_2 maintains well with the original ReS_2 structure. However, peaks belonging to Re_2O_7 decrease significantly with the continuous adding of Ce, possibly because adding Ce promotes the separation of ReS_2 nanosheets [25]. Moreover, Raman results (Fig. S2) also show a decreasing intensity of Re–O after introducing Ce.

Transmission electron microscopy (TEM) and high-resolution TEM (HRTEM) analyses are adopted to study the microscopic morphology of the as-synthesized electrocatalysts. In Fig. 1a–b, bare ReS_2 exhibits a poor microscopic morphology of nanosheets. For pure ReS_2 sample (Fig. 1c), several lattice interlayers of 0.26 nm belonging to ReS_2 (131), 0.61 nm ascribing to ReS_2 (001) and 0.33 nm assigning to Re_2O_7 (130) are acquired [26–28]. For the 1%Ce-ReS_2 sample, a distinct ultrathin morphology of ReS_2 is observed in Fig. 1d, which may favor electron transfer. From the high-resolution image in Fig. 1f, 1%Ce-ReS_2 shows a curly, similar lattice fringe belonging to ReS_2, while Re_2O_7 can hardly

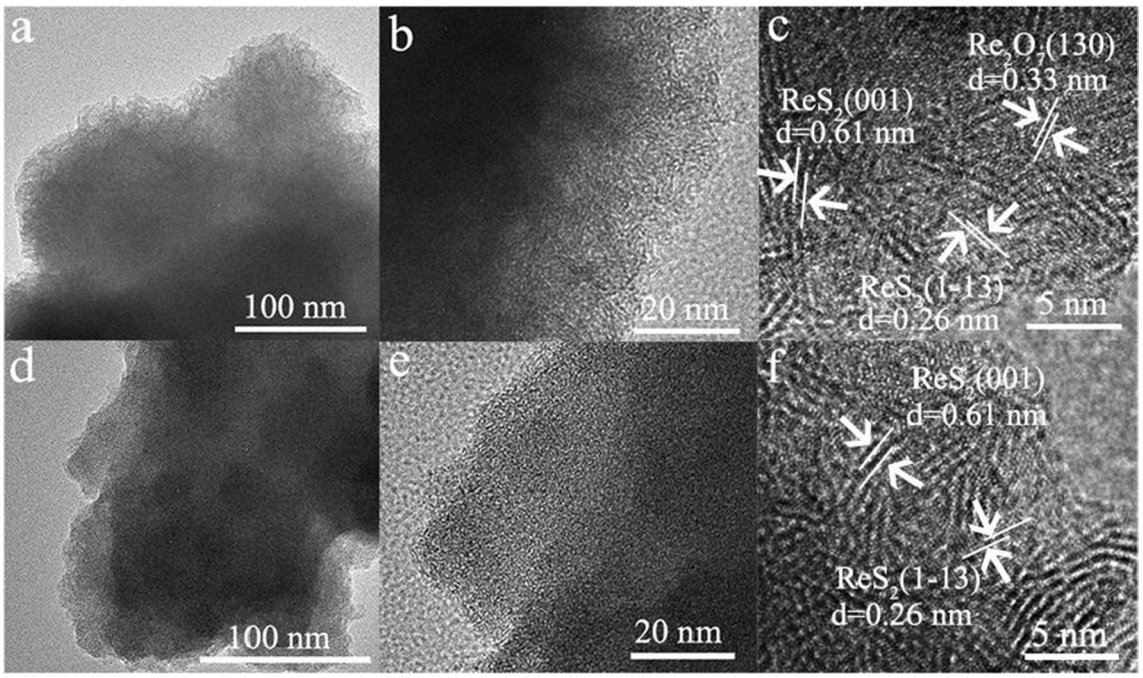

Fig. 1 TEM and HRTEM images of **a**–**c** pure ReS_2 and **d**–**f** 1%Ce-ReS_2 samples

be detected after adding Ce, and the results are consistent with XRD results.

The surface chemical composition and valence state of the elements in ReS_2 and 1%Ce-ReS_2 catalysts were tested by X-ray photoelectron spectroscopy (XPS). As shown in Fig. 2a, Ce, Re and S elements can all be detected in the survey scan. In Fig. 2b, peaks at 42.2 eV are ascribed to Re $4f_{7/2}$, and 44.5 eV matches well with Re $4f_{5/2}$, proving the successful

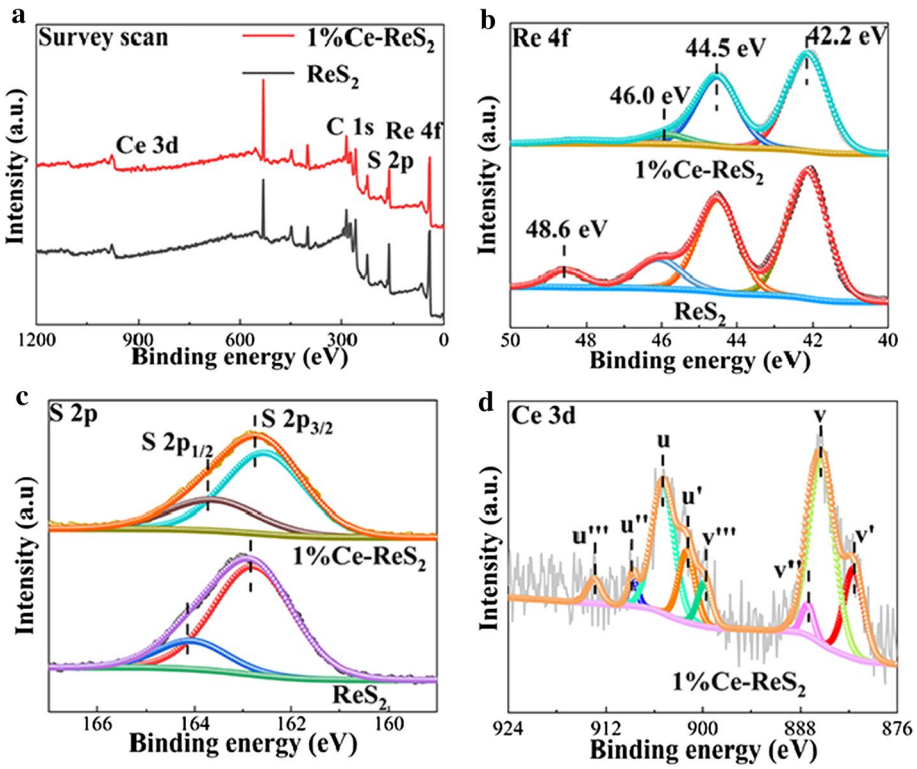

Fig. 2 X-ray photoelectron spectra of pure ReS_2 and 1%Ce-ReS_2 samples. **a** Survey scan, high-resolution signals of **b** Re 4f, **c** S 2p and **d** Ce 3d

preparation of ReS_2 [29]. Peaks at 46.0 eV and 48.6 eV belong to the Re^{7+} species [30]. However, the intensity of the peak at 46.0 eV decreased. Meanwhile, peak at binding energy of 48.6 eV disappeared after introducing Ce. These results are consistent with the above results. In Fig. 2c, peaks located at 162.8 eV and 164.1 eV are ascribed to S $2p_{3/2}$ and S $2p_{1/2}$ [31], respectively. The S $2p_{3/2}$ peak represents the metal–S bond, based on previous works [32, 33]. An obvious shift is observed after introducing of Ce, testifying to be newly formed S–metal (Ce–S) bond. According to the XPS results, the percentage of S $2p_{3/2}$ in S 2p is 81.2% for pure ReS_2 and 90.0% for the 1%Ce-ReS_2 sample. The above results demonstrate the formation of S-Ce after introducing Ce. For Ce 3d (Fig. 2d), peaks at binding energies of 913.6 eV (*u*'''), 908.8 eV (*u*''), 900.9 eV (*u*'), 899.8 eV (*v*'''), 887.3 eV (*v*'') and 881.5 eV (*v*') belong to Ce^{4+}, while peaks at 904.9 eV (*u*) and 885.7 eV (*v*) are assigned to Ce^{3+} [34]. For O 1 s XPS (Fig. S3), less Re_2O_7 can be detected after adding Ce, and this result is in accordance with the XRD and Raman results.

Electron spin resonance spectroscopy (ESR) characterization is used to study the defects of the ReS_2 and 1%Ce-ReS_2 electrocatalysts (Fig. 3). Clearly, the 1%Ce-ReS_2 electrocatalyst shows an enhanced result compared to bare ReS_2 ($g=2.00$) belongs to S defects [35], indicating that more defects were formed by introducing cerium. Generation of S defects contributed to a quasi-periodic atomic arrangement, which resulted in a slight rotation among mutual fringes. Additionally, the rearrangement of S and Re led to cracks on basal planes, resulting in the exposure of more reaction active sites and promoting hydrogen evolution performance [1].

Linear sweep voltammetry (LSV) is adopted to evaluate the hydrogen evolution activity of bare ReS_2 and *x*%Ce-ReS_2 samples (Fig. 4a). Pt/C is compared and exhibits remarkable HER performance (Fig. S4). Compared to bare ReS_2, *x*%Ce-ReS_2 composites display enhanced HER activity. In particular, 1%Ce-ReS_2 electrocatalyst obtains 10 mA/cm^2 at 306 mV compared to ReS_2 at more than 600 mV. In Fig. 4b, bare ReS_2 exhibits a Tafel plot of 268 mV/dec, whereas *x*%Ce-ReS_2 electrocatalysts (Fig. S5) show decreased ones. Notably, 1%Ce-ReS_2 shows the lowest Tafel plot of 99 mV/dec, which indicates that adding Ce contributed to the kinetics of hydrogen evolution. Generally, hydrogen evolution in an acid electrolyte includes Volmer, Heyrovsky and Tafel reactions [36] for the conversion of H^+ to H_2.

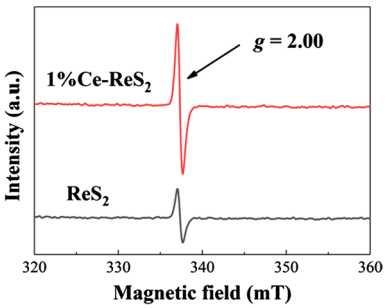

Fig. 3 Electron spin resonance spectroscopy of pure ReS_2 and 1%Ce-ReS_2 samples

Each of the reaction step requires different Tafel plots of 120, 40 and 30 mV/dec to occur. Therefore, the Tafel plot of 1%Ce-ReS_2 is 99 mV/dec, signifying that Volmer–Heyrovsky is the rate-limiting step in the HER. Adding Ce formed defects, which benefited reducing the adsorption energy of H_{ads}, which could greatly promoted HER performance. The obtained HER results of *x*%Ce-ReS_2 samples are compared with those of previously reported ReS_2-based electrocatalysts in Table S2. Introducing of Ce generated more S defects. Generation of S defects contributed to a quasi-periodic atomic arrangement, which resulted in a slight rotation among mutual fringes. Additionally, the rearrangement of S and Re may lead to cracks on basal planes, resulting in the exposure of more reaction active sites and promoting hydrogen evolution performance [1]. Generating more defects facilitated the reaction dynamics of the HER. Moreover, introducing cerium may promote the Volmer step and change the rate-limiting step from hydrogen adsorption to desorption and thus enhance the HER performance.

Additionally, the durability of the 1%Ce-ReS_2 was also tested and is shown in Fig. 4c, d. Obviously, the potential keeps a similar trend in long-term chronopotentiometry measurement. On the basis of CV results, the polarization curve of 1%Ce-ReS_2 after 1500 CVs identifies well with the original one, which testifies to the superior stability of 1%Ce-ReS_2 electrocatalyst. Furthermore, characterization of electrochemical surface areas (ECSAs) was studied (Fig. 4e). The C_{dl} of 1%Ce-ReS_2 is 3.8 mF/cm^2, while the C_{dl} of bare ReS_2 is 0.15 mF/cm^2 according to Fig. S6. The increased C_{dl} value signifies that more vacancy defects have been generated, exposing more reaction active sites and thus promoting the HER performance. Electrochemical impedance spectroscopy (EIS) was carried out to test the electroconductivity of bare ReS_2 and *x*%Ce-ReS_2 electrocatalysts (Figs. 4f and S7). Pure ReS_2 has larger Nyquist plots, while *x*%Ce-ReS_2 catalysts possess reduced resistance. A smaller resistance indicates better electron transfer. The above results illustrate that adding Ce exposed more active sites and accelerated electron transfer.

The *x*%Ce-ReS_2 samples also show a greatly promoted HER performance in an alkaline electrolyte (1 mol/L KOH). Compared to ReS_2, the HER performance of the *x*%Ce-ReS_2 electrocatalyst presents an evident promotion according to the LSV results in Fig. S8. Moreover, the durability of the 1%Ce-ReS_2 in 1 mol/L KOH was also tested and is exhibited in Fig. S9. Obviously, 1%Ce-ReS_2 electrocatalyst possesses superior stability.

In brief, a developed molten salt approach was adopted to construct Ce-modified ReS_2 electrocatalysts. The

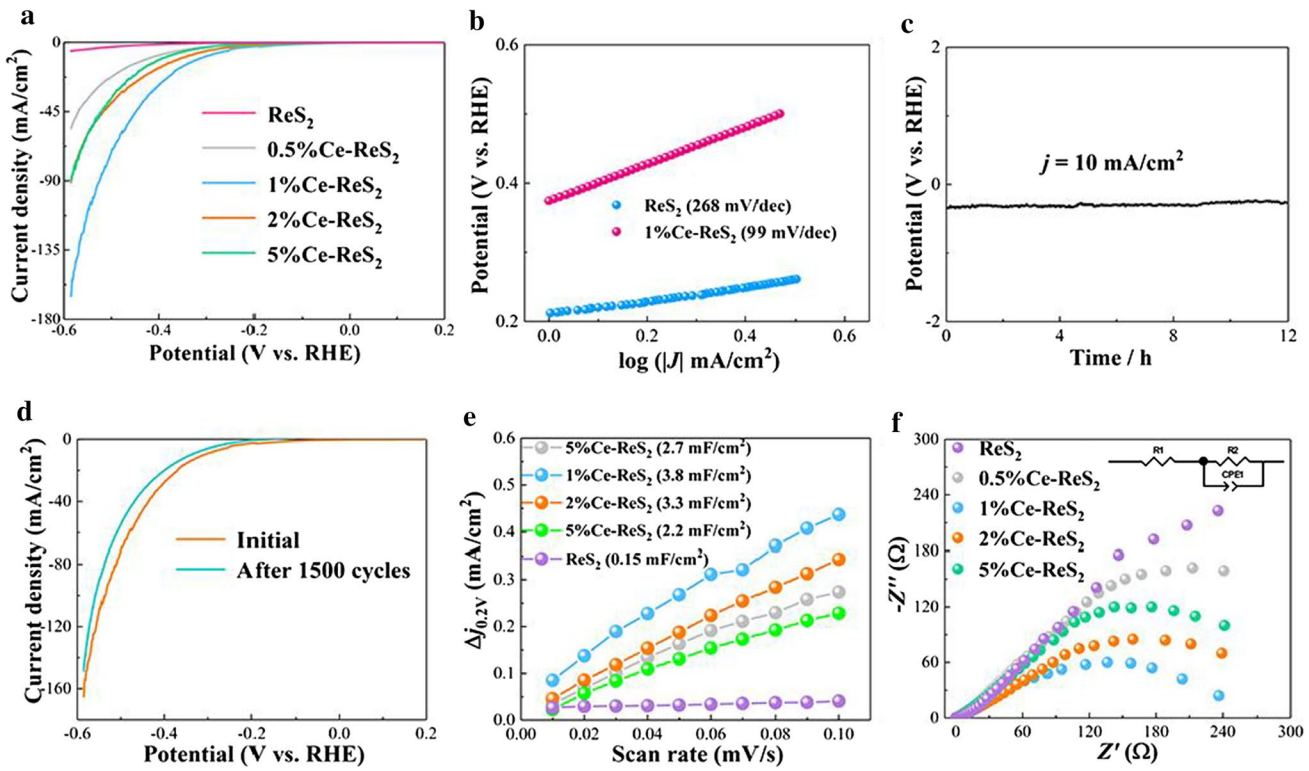

Fig. 4 **a** Polarization curves of pure ReS_2 and a series of x%Ce-ReS_2 electrocatalysts in 0.5 mol/L H_2SO_4; **b** Tafel plots from the corresponding LSV curves; **c** chronoamperometric spectra of the 1%Ce-ReS_2 sample at a constant current density of 10 mA/cm^2; **d** LSV curves of the 1%Ce-ReS_2 for the initial and 1500 CV cycles; **e** the capacitive current at 0.2 V as a function of scan rate for 1%Ce-ReS_2; **f** electrochemical impedance spectroscopy (EIS) Nyquist plots for pure ReS_2 and 1%Ce-ReS_2 samples

as-prepared x%Ce-ReS_2 electrocatalysts demonstrated greatly enhanced hydrogen evolution performance and excellent stability in acid electrolytes. Generating abundant defects in ReS_2 results in the exposure of more active sites. Meanwhile, introducing cerium contributes to the Volmer step and changes the rate-limiting step. Hopefully, these findings will offer new inspiration in designing efficient ReS_2-based electrocatalysts via the molten salt strategy.

Supplementary Information The online version contains supplementary material available at https://doi.org/10.1007/s12209-022-00314-1.

Acknowledgements This work was supported by Talent Program of Huangshan University (No. 2020xkjq010), Bureau of Huangshan Ecological Environment (No. hkxt2021212) and Key Project of Natural Science Research in Anhui Universities (No. KJ2020A0690), Major Project of Natural Science Research in Anhui Universities (No. KJ2019ZD42).

Declarations

Conflict of interest The authors declare that there is no conflict of interests.

References

1. Chen R, Ao YH, Wang C et al (2020) The surface engineering of ReS_2 with cobalt for efficient performance in hydrogen evolution under both acid and alkaline conditions. Chem Commun 56(60):8472–8475
2. Zhou TH, Wang DP, Chun-Kiat Goh S et al (2015) Bio-inspired organic cobalt(ii) phosphonates toward water oxidation. Energy Environ Sci 8(2):526–534
3. Fu Y, Shan Y, Zhou G et al (2019) Electric strain in dual metal Janus nanosheets induces structural phase transition for efficient hydrogen evolution. Joule 3(12):2955–2967

4. Liu MR, Hong QL, Li QH et al (2018) Cobalt boron imidazolate framework derived cobalt nanoparticles encapsulated in B/N codoped nanocarbon as efficient bifunctional electrocatalysts for overall water splitting. Adv Funct Mater 28(26):1801136
5. Xiao FX, Liu B (2017) In situ etching-induced self-assembly of metal cluster decorated one-dimensional semiconductors for solar-powered water splitting: unraveling cooperative synergy by photoelectrochemical investigations. Nanoscale 9(43):17118–17132
6. Li H, Tsai C, Koh AL et al (2016) Activating and optimizing MoS_2 basal planes for hydrogen evolution through the formation of strained sulphur vacancies. Nat Mater 15(1):48–53
7. Kiriya D, Lobaccaro P, Nyein HYY et al (2016) General thermal texturization process of MoS_2 for efficient electrocatalytic hydrogen evolution reaction. Nano Lett 16(7):4047–4053
8. Cai M, Zhang F, Zhang C et al (2018) Cobaloxime anchored MoS_2 nanosheets as electrocatalysts for the hydrogen evolution reaction. J Mater Chem A 6(1):138–144
9. Wu ZZ, Fang BZ, Bonakdarpour A et al (2012) WS_2 nanosheets as a highly efficient electrocatalyst for hydrogen evolution reaction. Appl Catal B Environ 125:59–66
10. Cheng L, Huang WJ, Gong QF et al (2014) Ultrathin WS_2 nanoflakes as a high-performance electrocatalyst for the hydrogen evolution reaction. Angew Chem Int Ed Engl 53(30):7860–7863
11. Lukowski MA, Daniel AS, English CR et al (2014) Highly active hydrogen evolution catalysis from metallic WS_2 nanosheets. Energy Environ Sci 7(8):2608–2613
12. Zhang YJ, Gong QF, Li L et al (2015) $MoSe_2$ porous microspheres comprising monolayer flakes with high electrocatalytic activity. Nano Res 8(4):1108–1115
13. Wang XQ, Chen YF, Zheng BJ et al (2016) Few-layered WSe_2 nanoflowers anchored on graphene nanosheets: a highly efficient and stable electrocatalyst for hydrogen evolution. Electrochim Acta 222:1293–1299
14. Keyshar K, Gong YJ, Ye GL et al (2015) Chemical vapor deposition of monolayer rhenium disulfide (ReS_2). Adv Mater 27(31):4640–4648
15. Qi F, He JR, Chen YF et al (2017) Few-layered ReS2 nanosheets grown on carbon nanotubes: a highly efficient anode for high-performance lithium-ion batteries. Chem Eng J 315:10–17
16. Ovchinnikov D, Gargiulo F, Allain A et al (2016) Disorder engineering and conductivity dome in ReS_2 with electrolyte gating. Nat Commun 7:12391
17. Xu XY, Zhao H, Wang R et al (2018) Identification of few-layer ReS_2 as photo-electro integrated catalyst for hydrogen evolution. Nano Energy 48:337–344
18. Gao H, Yue HH, Qi F et al (2018) Few-layered ReS_2 nanosheets grown on graphene as electrocatalyst for hydrogen evolution reaction. Rare Met 37(12):1014–1020
19. Fujita T, Ito Y, Tan YW et al (2014) Chemically exfoliated ReS_2 nanosheets. Nanoscale 6(21):12458–12462
20. Wang M, Zhang L, Huang MR et al (2019) One-step synthesis of a hierarchical self-supported WS_2 film for efficient electrocatalytic hydrogen evolution. J Mater Chem A 7(39):22405–22411
21. Wang HX, Fu WW, Yang XH et al (2020) Recent advancements in heterostructured interface engineering for hydrogen evolution reaction electrocatalysis. J Mater Chem A 8(15):6926–6956
22. Yan CS, Zhu Y, Fang ZW et al (2018) Heterogeneous molten salt design strategy toward coupling cobalt-cobalt oxide and carbon for efficient energy conversion and storage. Adv Energy Mater 8(23):1800762
23. Yamada M, Tago M, Fukusako S et al (1993) Melting point and supercooling characteristics of molten salt. Thermochim Acta 218:401–411
24. Nan KK, Du HF, Su L et al (2018) Directly electrodeposited cobalt sulfide nanosheets as advanced catalyst for oxygen evolution reaction. Chem Select 3(25):7081–7088
25. Chen XX, Zhai XW, Hou J et al (2021) Tunable nitrogen-doped delaminated 2D MXene obtained by NH_3/Ar plasma treatment as highly efficient hydrogen and oxygen evolution reaction electrocatalyst. Chem Eng J 420:129832
26. Lu XY, Liu RT, Wang Q et al (2019) In situ integration of ReS_2/Ni_3S_2 p-n heterostructure for enhanced photoelectrocatalytic performance. ACS Appl Mater Interfaces 11(43):40014–40021
27. Zhang Q, Tan SJ, Mendes RG et al (2016) Extremely weak van der waals coupling in vertical ReS_2 nanowalls for high-current-density lithium-ion batteries. Adv Mater 28(13):2616–2623
28. Skosyrev NT, Spivak MM, Sapukov IA (1985) The X-Ray powder diffraction pattern of rhenium (VII) oxide. Russ J Inorg Chem 30:1695
29. Qi F, Chen YF, Zheng BJ et al (2017) Hierarchical architecture of ReS_2/rGO composites with enhanced electrochemical properties for lithium-ion batteries. Appl Surf Sci 413:123–128
30. Liu LJ, Asano T, Nakagawa Y et al (2019) Selective hydrogenolysis of glycerol to 1,3-propanediol over rhenium-oxide-modified iridium nanoparticles coating rutile titania support. ACS Catal 9(12):10913–10930
31. Zhou G, Guo ZJ, Shan Y et al (2019) High-efficiency hydrogen evolution from seawater using hetero-structured T/Td phase ReS_2 nanosheets with cationic vacancies. Nano Energy 55:42–48
32. Gao MR, Liang JX, Zheng YR et al (2015) An efficient molybdenum disulfide/cobalt diselenide hybrid catalyst for electrochemical hydrogen generation. Nat Commun 6:5982
33. Lin JH, Wang PC, Wang HH et al (2019) Defect-rich heterogeneous MoS_2/NiS_2 nanosheets electrocatalysts for efficient overall water splitting. Adv Sci (Weinh) 6(14):1900246
34. Chen R, Chen J, Gao X et al (2021) Probing the role of surface acid sites on the photocatalytic degradation of tetracycline hydrochloride over cerium doped CdS via experiments and theoretical calculations. Dalton Trans 50(45):16620–16630
35. Zhang YL, Mu ZJ, Yang C et al (2018) Rational design of MXene/1T-2H MoS_2-C nanohybrids for high-performance lithium-sulfur batteries. Adv Funct Mater 28(38):1707578
36. Ji LL, Lv CC, Chen ZF et al (2018) Nickel-based (photo)electrocatalysts for hydrogen production. Adv Mater 30(17):e1705653

Dr. Ran Chen has been a faculty member at Huangshan University, Anhui Province, since 2021. He received his PhD at Hohai University, Jiangsu Province, in 2021. His research interests focus on photocatalysis, electrocatalysis and thermocatalysis.